Stochastic scanning multiphoton multifocal microscopy

Justin E. Jureller, Hee Y. Kim and Norbert F. Scherer

Department of Chemistry and Institute for Biophysical Dynamics, The University of Chicago
5735 South Ellis Ave, Chicago, IL 60637
nfschere@uchicago.edu

Abstract: Multiparticle tracking with scanning confocal and multiphoton fluorescence imaging is increasingly important for elucidating biological function, as in the transport of intracellular cargo-carrying vesicles. We demonstrate a simple rapid-sampling stochastic scanning multiphoton multifocal microscopy (SS-MMM) fluorescence imaging technique that enables multiparticle tracking without specialized hardware at rates 1,000 times greater than conventional single point raster scanning. Stochastic scanning of a diffractive optic generated 10x10 hexagonal array of foci with a white noise driven galvanometer yields a scan pattern that is random yet space-filling. SS-MMM creates a more uniformly sampled image with fewer spatio-temporal artifacts than obtained by conventional or multibeam raster scanning. SS-MMM is verified by simulation and experimentally demonstrated by tracking microsphere diffusion in solution.

OCIS codes: (180.5810) Scanning microscopy; (180.1790) Confocal microscopy; (180.2520) Fluorescence microscopy; (050.1970) Diffractive optics; (110.0180) Microscopy

References and links

1. V. Levi, Q. Ruan, and E. Gratton, "3-D particle tracking in a two-photon microscope: application to the study of molecular dynamics in cells," Biophys. J. **88**, 2919-2928 (2005).
2. W. Denk, J. H. Strickler, and W. W. Webb, "Two-photon laser scanning fluorescence microscopy," Science **248**, 73-76 (1990).
3. K. Kim, C. Buehler, and P. So, "High-speed, two-photon scanning microscope," Appl. Opt. **38**, 6004-6009 (1999).
4. A. Diaspro, *Confocal and two-photon microscopy* (Wiley, New York, 2002).
5. M. A. Digman, C. M. Brown, P. Sengupta, P. W. Wiseman, A. R. Horwitz, and E. Gratton, "Measuring fast dynamics in solutions and cells with a laser scanning microscope," Biophys. J. **89**, 1317-1327 (2005).
6. J. Bewersdorf, R. Pick, and S. W. Hell, "Multifocal multiphoton microscopy," Opt. Lett. **23**, 655-657 (1998).
7. V. Andresen, A. Egner, and S. W. Hell, "Time-multiplexed multifocal multiphoton microscope," Opt. Lett. **26**, 75-77 (2001).
8. D. N. Fittinghoff and J. A. Squier, "Time-decorrelated multifocal array for multiphoton microscopy and micromachining," Opt. Lett. **25**, 1213-1215 (2000).
9. L. Sacconi, E. Froner, R. Antolini, M. R. Taghizadeh, A. Choudhury, F. S. Pavone, "Multiphoton multifocal microscopy exploiting a diffractive optical element," Opt. Lett. **28**, 1918-1920 (2003).
10. K. C. Toussaint Jr., S. Park, J. E. Jureller and N. F. Scherer, "Generation of optical vector beams using a diffractive optical element interferometer," Opt. Lett. **30**, 2846-2848 (2005).
11. V. Levi, Q. Ruan, and E. Gratton, "3-d particle tracking in a two-photon microscope: application to the study of molecular dynamics in cells," Biophys. J. **88**, 29192928 (2005).
12. R. Jin, J. E. Jureller, H. Y. Kim, and N. F. Scherer, "Correlating second harmonic optical responses of single Ag nanoparticles with morphology," J. Amer. Chem. Soc. **127**, 12482-12483 (2005).
13. A. Egner and S. W. Hell, "Time multiplexing and parallelization in multifocal multiphoton microscopy," J. Opt. Soc. Am. A **17**, 1192-1201 (2000).

#68197 - $15.00 USD Received 28 February 2006; revised 11 April 2006; accepted 12 April 2006

14. J. C. Crocker and D. G. Grier. "Methods of digital video microscopy for colloidal studies," J. Coll. Inter. Sci. **179**, 298310 (1996).
15. J. E. Jureller, "Nonlinear and correlation microscopies for dyanmics and function in heterogeneous systems," Ph.D. Dissertation, The University of Chicago (2006).
16. J. E. Jureller, H. Y. Kim, L. Ma, A. Kuznetsov, L. H. Philipson and N. F. Scherer, are preparing a manuscript entitled "Vesicular transport measured with stochastic scanning multiphoton multifocal microscopy."

1. Introduction

Measuring transport dynamics in temporally and spatially heterogenous nano- and micro-scale systems (e.g. cargo vesicles *in vivo*) requires high-resolution and high-fidelity concurrent tracking of individual objects over large fields of view.[1] Laser scanning confocal or multiphoton fluorescence imaging microscopies are powerful approaches for imaging and tracking.[2, 3, 4] Moreover, rapid scanning rates are required to avoid spatiotemporal artifacts in the measured sample dynamics arising from the laser scanning spatial response function.[1, 5] Systems with the requisite capabilities, particularly those with spinning discs or resonant galvanometers, are often expensive, specialized, and closed "black boxes" that hinder operator innovation.

Consider a raster laser scanning multiphoton fluorescence microscopy imaging process with a (nonresonant) galvanometer and nondescanned detection: sweeping an excitation spot or pattern over a sample area in the conjugate plane of a array detector produces an image. The detector exposure time must be synchronized to the period of the raster scanner slow axis drive waveform. This introduces an asymmetry: the fast axis is continuously sampled while the slow axis is discretely sampled. Raster scanning utilizes only a portion of the possible scanning power spectral bandwidth, limiting full-field imaging rates to a few frames per second. Furthermore, no information is available about an area of a sample while the excitation beam is elsewhere. Temporal and spatial aliasing artifacts appear for processes with timescales comparable to or faster than the full frame rate and are especially severe across wide fields of view. While generally undesirable for imaging or multi-particle tracking, these "artifacts" have been employed as a correlation spectroscopy.[5]

Multifocal multiplexing increases scanning efficiency by using two-dimensional patterns of excitation spots that need only be dithered within the periodic bounds of the array.[6] Initial implementations of multiphoton multifocal microscopy (MMM) utilized microlenses,[6, 7] cascaded beamsplitter arrays,[8] and low-spot-density diffractive optical elements (DOE) to generate excitation patterns.[9] DOE beamsplitters offer compactness, stability, efficiency, and uniformity. [10] DOE throughput ($\sim$75%) is similar to microlens arrays without pinholes and allows producing a large number of beams ($\sim$100) with uniform intensity ($<$5% peak-to-peak variation). However, previous designs relied on conventional rastering and lead to oversampling at the edges of each unit cell due to the finite mechanical response of the scanner. Hence, the resulting images exhibited a gridwork appearance. Nipkow spinning disk scanners do not exhibit this effect,[6, 7] but are restricted to non-random access movements. It is desirable to maintain flexibility for the utilization of random access scanning modes such as have been recently employed for measurement of intracellular transport.[11]

We demonstrate a simple rapid sampling stochastic scanning multiphoton multifocal microscopy (SS-MMM) approach that addresses these shortcomings. SS-MMM enables high-speed uniform imaging and allows high-fidelity multiparticle tracking. The method entails using a DOE to generate a 10x10 excitation beam array arranged in a hexagonal lattice. This uniform intensity array yields 100 beam foci at the objective focal plane that are scanned by a galvanometer. Instead of driving the galvo with a conventional raster waveform, it is driven by a "white noise" waveform resulting in a random scanning motion. Therefore, "stochastic scanning" should be thought of as an image sampling process akin to a Brownian random walk in two-dimensions. The image is sampled and "built-up" within a given integration time that de-

#68197 - $15.00 USD Received 28 February 2006; revised 11 April 2006; accepted 12 April 2006

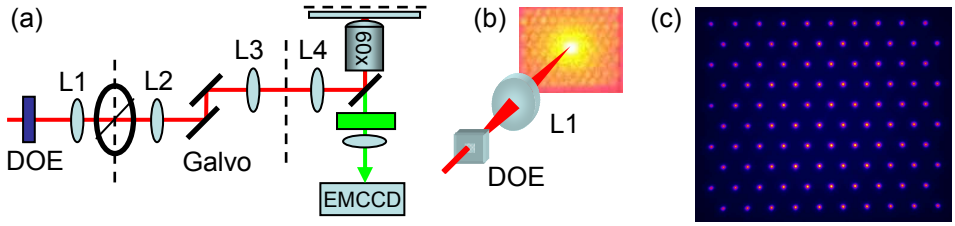

Fig. 1. (a) SS-MMM setup. (b) DOE generated 10x10 hexagonal multifocal array. The smaller image is the actual array after L1. (c) False color two-photon fluorescence image of the multifocal array in a solution of Rhodamine 6G at the sample plane.

termines the overall image fidelity, rather than a set frame rate. The resulting images are evenly and symmetrically sampled and allow full-field scanning with asynchronous frame readout (i.e. the detector and scan are not synchronized) 1000 times greater than conventional single beam rastering. Expensive specialized equipment is avoided as well as artificial duty-cycle inefficiencies designed to account for unequal mechanical scanner residency times (e.g. electrooptic beam-blanking of the excitation at the edges of the scan waveform). Therefore, the ultimate imaging and tracking rates are determined by the intrinsic fluorophore brightness, detector sensitivity and readout rate, not by the scanner. The experimental results are supported by Monte Carlo simulations of microsphere diffusion and SS-MMM imaging. We demonstrate our SS-MMM approach for high-resolution multiparticle tracking and imaging with multiphoton excitation for its deep confocality, low background, and reduced overall (primarily out-of-plane) photobleaching advantages. [2, 4] SS-MMM will therefore be a powerful technique for tracking intracellular cargo vesicles *in vivo*. Additionally, the SS method is general and adaptable to one-photon confocal descanned methods.

2. Experiment

The SS-MMM setup (Fig. 1) is based on a home-built nonlinear optical (i.e. 2-photon) microscope recently reported elsewhere.[12] Briefly, 70 fs duration pulses at 930 nm obtained from a tunable Ti:Sapphire laser (Spectra-Physics Mai Tai) are used to generate 2-photon fluorescence at the focal plane of a 1.2 NA 60x water immersion apochromat objective (Olympus UPLSAPO 60XW) mounted on an inverted microscope (Nikon TE2000E). After dispersion pre-compensation with a BK7 Brewster-cut prism line and cleanup of the beam with a spatial filter, the beam illuminates a binary DOE, custom made to our specifications (Holoeye AG) with a 20 cm focal length. This DOE produces a 10x10 hexagonal array of excitation beams, with a measured generation efficiency of 75% and $<$ 5% variation in beam intensity. The period of the two-dimensional diffraction grating comprising the DOE is 219 μm. The hexagonal geometry and resultant even inter-beam spacing allows optimal sampling and imaging efficiency. A telescope constructed with near-IR achromats (L1, f.l.=20 cm and L2, f.l.=35 cm) in a standard 4-f configuration images the DOE onto the face of the galvanometer scanner. The residual undiffracted beam is designed to occur in an interstitial space and is mechanically blocked with a wire at the focus of the telescope after lens L1, also the first conjugate plane of the sample plane (Fig. 1(b)).

The pattern is scanned across the field of view by a two-mirror closed-loop galvanometer (Cambridge Tech 6650) with a 286 Hz resonant frequency (selected for stability and accuracy) driven by triangular raster or white noise waveforms synthesized by a NI-6052E DAQ card. In raster scan mode, fast axis scan rates must be limited to under 100 Hz to avoid mechanical lags and therefore the overall imaging rates (slow axis) are limited to 1-2 fps. Stochastic scanning

#68197 - $15.00 USD Received 28 February 2006; revised 11 April 2006; accepted 12 April 2006

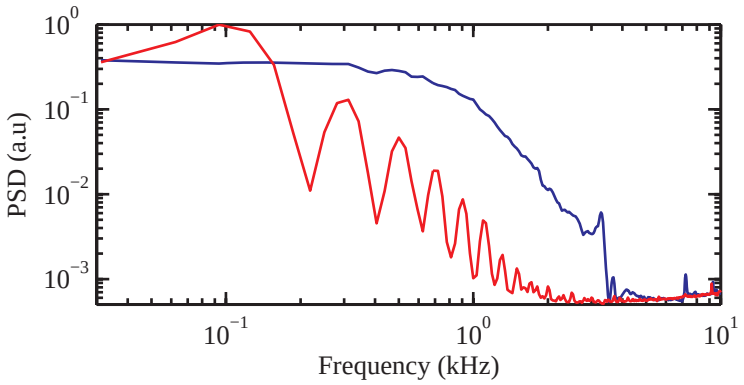

Fig. 2. Log-log plot of the measured galvanometer response power spectral density driven by white noise (blue) and 100 Hz raster (red) waveforms.

imaging rates are not limited in this way. The optical train is completed with a near-IR achromat scan lens (L3, f.l.= 15 cm) and tube lens (L4, f.l.=20 cm) leading to the primary objective. Generated multiphoton fluorescence is epi-detected, separated from the scattered laser light with a green HQ525/50m bandpass filter and E700SP2 NIR blocking filter (Chroma). Epi-fluorescence is imaged onto a 1000x1000 pixel TE-cooled EMCCD camera (Andor DV885) with 100x total magnification. Effective back-projected pixels are 80 nm square. Fig. 1(c) shows a false color 2-photon fluorescence image of the hexagonal array of excitation foci at the sample focal plane in a solution of Rhodamine 6G. Foci are separated by 6 μm to prevent adverse interference effects.[13] The average power of the pattern is adjustable with neutral density filters so that individual foci at the sample plane have 0.5-10 mW each.

SS-MMM is experimentally demonstrated by measuring the diffusion of 500 nm diameter yellow-green fluorescent microspheres (Duke) in aqueous solution between two coverslips separated by a 100 μm gasket.The Stokes-Einstein relation gives an expected diffusion coefficient $D = 0.88\ \mu\text{m}^2/\text{s}$.[14]

3. Results and Discussion

The galvanometer response power spectral density measured with a spectrum analyzer (SRS SR760) is shown in Fig. 2. The red curve results from a 100 Hz raster scan drive waveform while the blue curve results from a white noise drive waveform that utilizes the full 333 KHz bandwidth of the DAQ. This latter response is pertinent for SS-MMM and reflects the total mechanical bandwidth available from this galvo. It is substantially flatter and extends to much higher frequencies than the raster response. The odd harmonic components of the raster response result from the approximation of a triangular wave drive waveform, with dominant contributions from the edges of the trajectory, i.e the reversal points. Triangular drive waveforms are preferred to simple square and step drive waveforms due to the minimization of stop-start impulses to the scanner. Stochastic scanning enables high-frequency content at all points in the scan pattern. Therefore stochastic scanning is mechanically more efficient than rastering at a sub-resonant frequency. Fig. 3(a) shows a single frame 2-photon fluorescence image of a monolayer of 500 nm diameter fluorescent microspheres acquired with raster scanning at 1 fps. Boundaries between periodic replica cells are clearly over-sampled and are observed as bright edges of the single beam scan area. The slow axis edges (horizontal) are deemphasized versus the fast axis edges (vertical), but still noticeable for this galvanometer. Fig. 3(b) shows a single frame 2-photon fluorescence image of the same area obtained by stochastic scanning. The

#68197 - $15.00 USD Received 28 February 2006; revised 11 April 2006; accepted 12 April 2006

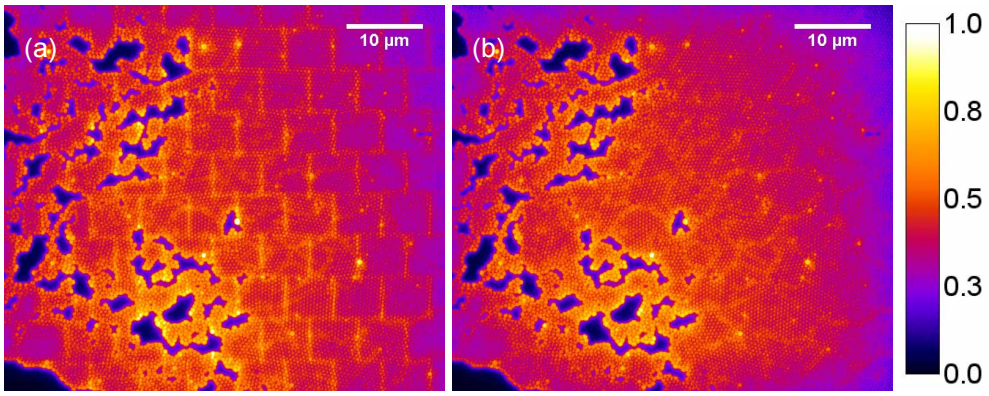

Fig. 3. (a) Single frame two-photon fluorescence multifocal raster scan image of a packed monolayer of 500 nm diameter microspheres at 1 fps. The unit cell boundaries are clearly oversampled, yielding artifacts in a brickwork pattern. (b) Single frame SS-MMM fluorescence image of the same area. The brickwork artifacts in (a) are not observed.

sampling is much more uniform and the image does not display the edge sampling artifacts. This relatively slow imaging rate (1 fps) represents the best-case-scenario for raster scanning; imaging at faster rates will only increase the observed artifacts.

The DOE acts as a spectrally dispersive element that can spatially broaden the foci at the sample focal plane. Calculated spatial dispersion of the 10 nm spectral bandwidth pulses ranges from 91 nm FWHM for the 1st order spots to 460 nm FWHM for the highest order spots at the pattern edge.[9] This estimate includes a 2.3x magnification of the DOE from the two telescopes (L1, L2, L3 and L4). These values are less than the 460 nm FWHM linear diffraction-limited illumination focus for the 930 nm excitation pulses and would create a $< \sqrt{2}$ increase in a spot size at the pattern's edge. The overall effect would be to decrease the instantaneous peak power found in the foci, and therefore reduced 2-photon fluorescence. In practice, this effect was small, but noticeable at the edge of the pattern. Identical reductions in intensity toward the edge of the image are observed for both raster and stochastic scanning in Fig. 3.

A greater reduction at the very edges of the stochastic scanning full field of view reflects the reduced illumination resulting from the outermost unit cells of the scan pattern where the next unit cell does not exist and cannot contribute to smoothing the pattern boundaries. The central 8x8 (even 9x9) pattern region of the images are very uniformly illuminated.

Monte Carlo simulations (written in Matlab) of the imaging process were undertaken to better quantify the SS-MMM technique. Experimental parameters (e.g. the galvo mechanical response, pixel size, beam waist, excitation spot spacing and field of view) are included to yield realistic data that were validated by direct comparison to experimental measurements. Full details are reported elsewhere.[15, 16] As a practical consideration, the 10 MHz readout rate of the particular EMCCD used limits experimental non-binned full-frame acquisition rates to 9 fps. SS-MMM is capable of higher frame rates (video and beyond) and the simulations allow modeling these conditions and extrapolation to higher imaging rates. In practice these rates would be achieved with a faster detector or detection of only a sub-area with this camera but at the expense of the large field of view covered by the excitation array.

Fig. 4(a and b) show histograms of calculated fast axis pixel residence times within one unit of the periodic multifocal array for raster (a) and stochastic (b) scans at 1 fps. Both axes are sampled equivalently rapidly for stochastic scanning with a bandwidth advantage as stated above. Raster scanning clearly oversamples the edges even at low speeds. Stochastic scanning

#68197 - $15.00 USD Received 28 February 2006; revised 11 April 2006; accepted 12 April 2006

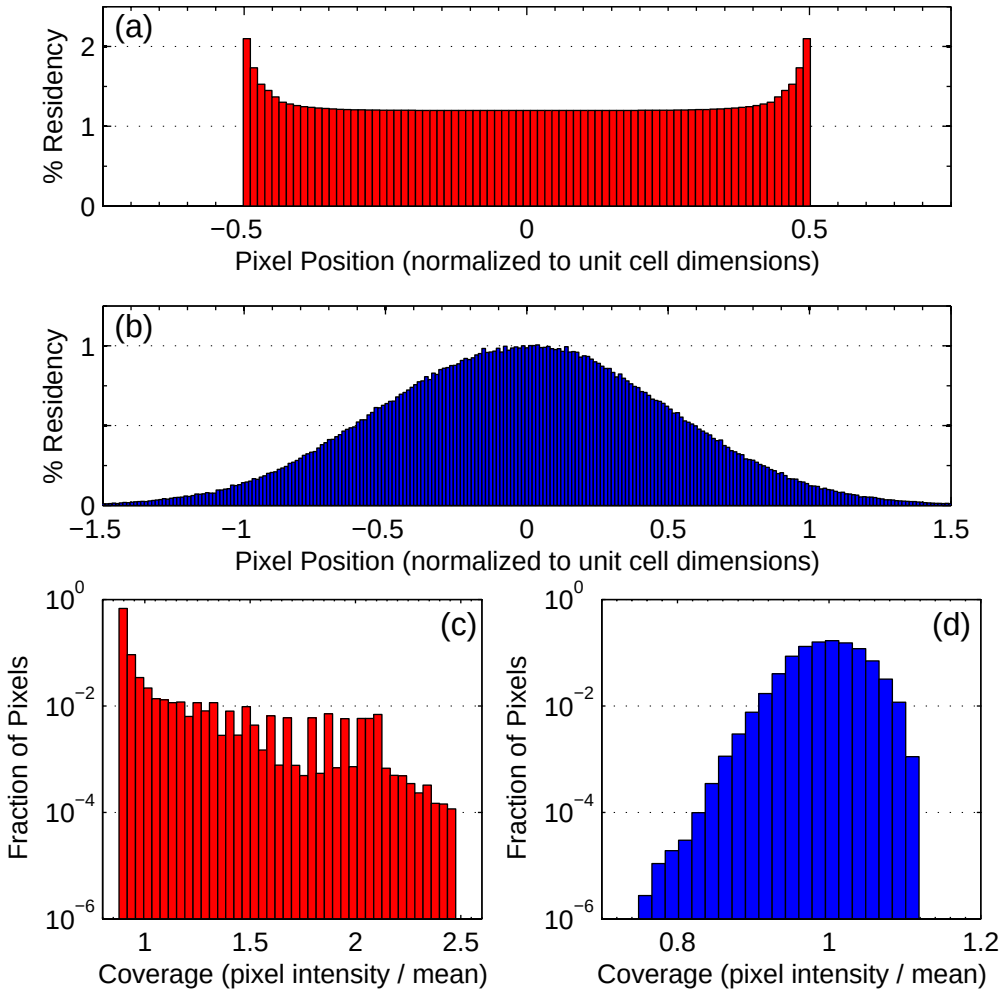

Fig. 4. Histograms (bin width = 1 pixel) of simulated fast axis residency times in units of array spacing at 1 fps for (a) raster and (b) stochastic scanning. (c and d) Histograms of scanning coverage (pixel intensities normalized by the mean image intensity) for simulated full images at 1 fps. (c) Raster scanning shows a broad distribution and large oversampling. (d) Stochastic scanning shows a much tighter distribution and a small undersampled tail.

yields nearly the inverse; the sampling is more uniform and mostly in the center of the unit cells. This is exactly what is required to form an evenly sampled composite image when combining contributions from each part of the excitation array. The excursions outside the array unit cell serve to better blend each area with its neighbors. Conversely, raster scanning oversamples the unit cell edge and results in a gridwork effect. This exemplifies the advantage of stochastic scanning over raster scanning, especially at higher (overdriven) frequencies.

A metric is needed to quantify the quality and extent of scanning "coverage," i.e. the distribution of total excitation dosage a given sample position or EMCCD pixel receives due to the beam scanning trajectory. The coverage may be quantified in a histogram of pixel intensity values in the scan region normalized by the value expected for completely uniform illumination; i.e. the mean pixel intensity averaged over the whole image. The histogram of a perfect,

#68197 - $15.00 USD Received 28 February 2006; revised 11 April 2006; accepted 12 April 2006

Table 1. Imaging simulation coverage results

Scan type	fps	Mean Intensity	Relative Std Dev
Stochastic	1000	0.047	1.17
Stochastic	100	0.278	0.362
Raster	100	0.129	0.801
Stochastic	10	0.692	0.115
Raster	10	0.537	0.154
Stochastic	1	0.901	0.040
Raster	1	0.407	0.257

uniformly covered scan pattern would yield a delta function at 1. The relative standard deviation of the coverage distribution, describing the width of the histogram, can then be calculated as the standard deviation of the pixel intensities divided by the mean intensity value. A narrow relative standard deviation indicates the uniformity of coverage. In this way, histograms for scan patterns with different mean values may be directly compared and quantify the smoothness and completeness of scanning coverage.

Fig. 4 shows histograms of coverage values calculated from images generated by simulations of multifocal (c) raster and (d) stochastic scanning trajectories at 1 fps. The areas of the histograms are normalized to one, so that the they may be read as the fraction of pixels with a given coverage. The width of the stochastic scanning histogram is much narrower and distributed around 1, indicating a high degree of image scanning uniformity. The raster histogram exhibits significant nonuniformity. The higher coverage values indicate some pixels are oversampled up to 2.5 times the average illumination. This is a signature of oversampling of the edges of the scan unit cell. The stochastic histogram does display a small tail of undersampling, resulting from the outermost edges of the scan pattern where the next unit cell to "blend" the coverage does not exist.

Table 1 gives the mean pixel intensities on a scale of zero to unity and the relative standard deviations of additional histogram distributions (not shown) at representative frame rates. For equivalent conditions, stochastic scanning produces more evenly sampled images with narrower distributions; i.e. the mean values are higher and the relative standard deviations are smaller. Importantly, all stochastically scanned pixels have non-zero values until frame rates exceed 100 fps. This means that the excitation beam illuminates each pixel and that there are no "holes" in the scanning trajectory. Beyond this rate (e.g. 1000 fps) there is a probability that a pixel will not be visited, creating a blinking effect from frame to frame. These temporal artifacts would be similar to those encountered with much slower ($\sim$ 1 fps) raster scans. Conservatively, estimating 100 fps as the limit of stochastic scanning with this galvanometer gives a 1,000-fold improvement over conventional single-beam rastering. A complete analysis is presented elsewhere.[15, 16]

Multiparticle tracking is an important application of such high-speed imaging. Fig. 5(a) shows a portion of an image of 500 nm diameter fluorescent microspheres diffusing in aqueous solution acquired at 9 fps with SS-MMM. Centroid particle tracking analysis of the images allows calculation of the mean square displacement (MSD). For two-dimensional diffusion (appropriate for bead trajectories that stay within the optically sectioned focal plane), the fitted slope of the MSD should equal $4D$. [14] Fig. 5(c) shows the measured average MSD (red circles) of the microspheres. A linear fit (solid) yields a diffusion coefficient of 0.87 $\mu m^2/s$, in very good agreement with the expected value of $D = 0.88$ μm^2/s.[14] Fig. 5(b) shows a simulated stochastic scanning image of 500 nm diameter fluorescent microspheres diffusing in

#68197 - $15.00 USD Received 28 February 2006; revised 11 April 2006; accepted 12 April 2006

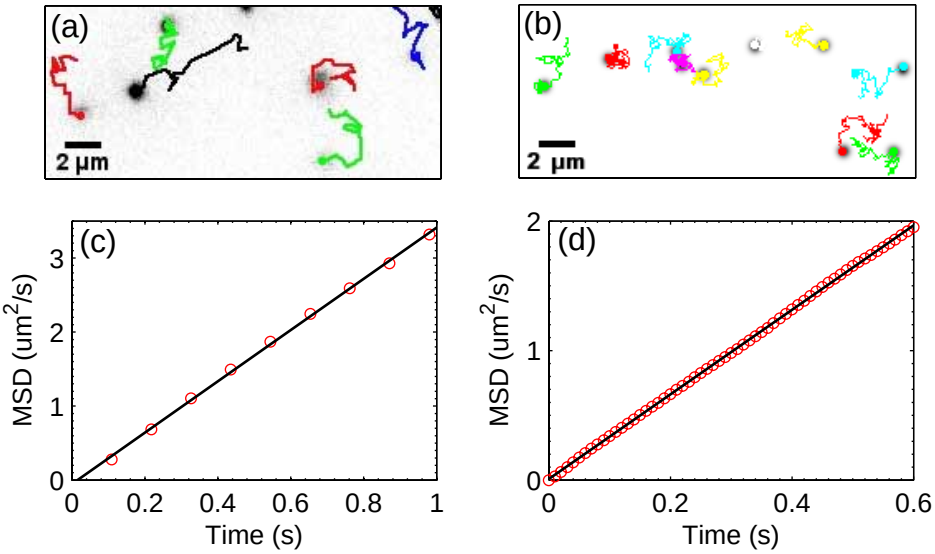

Fig. 5. (a) Representative experimental microsphere trajectories measured with SS-MMM at 9 fps and (b) simulated microsphere trajectories measured with SS-MMM at 100 fps. (c) MSD from the experimentally measured trajectories in (a) and linear fit (solid line). (d) MSD from the simulations in (b) and linear fit (solid line).

aqueous solution at 100 fps. The diffusion coefficient used in the Monte Carlo simulation was 0.82 μm^2. Fig. 5(d) shows the measured average MSD (red circles). A linear fit (solid) gives 0.82 μm^2 as the diffusion coefficient. Particle trajectories and transport are still measured with high fidelity at 100 fps, unreachable with conventional single beam raster scanning.

4. Conclusion

We have demonstrated a simple stochastic scanning multiphoton multifocal microscopy (SS-MMM) fluorescence technique designed for high-speed imaging and proven its utility for multiparticle tracking of fast dynamics over large fields of view. Spatial multiplexing and stochastic scanning are shown to work uniquely well and synergistically. The hexagonal array of 100 excitation foci generated from a DOE is the densest reported and likely constitutes the practical limit due to available laser power. Stochastically scanning the array provides enhancement in sampling bandwidth and imaging uniformity versus raster scanning. Instead of using a single frequency necessarily well below the resonant frequency, the entire galvanometer bandwidth may be used (with amplitude up to 3 kHz, 10x greater than the galvanometer resonant frequency). This approach allows $>$ 100-fold more temporal information to be obtained with more uniform coverage than simply overdriving a multifocal rastering waveform. The limit is rarefication of sampling, which leads to sparsity in the image or "blinking" of objects. No hardware or software synchronization of the scan pattern to the CCD pixel clock is required. Therefore, inexpensive equipment may be used without modification to achieve similar performance to expensive and sealed commercial systems.

SS-MMM is ideal for biological tracking applications such as measuring the transport of intracellular cargo vesicles. Extending SS-MMM to 3-D volume (and 4-D time) imaging is straightforward, but beyond the scope of this current paper where the focus is on the idea of rapid random access (stochastic) scanning for imaging and particle tracking. Such biologi-

#68197 - $15.00 USD Received 28 February 2006; revised 11 April 2006; accepted 12 April 2006

cal tracking and volumetric imaging studies with further characterization (e.g. axial resolution measurements) of the stochastic scanning method will be reported in a future paper. [16]

Acknowledgements

J.E.J acknowledges the support of a Burroughs-Wellcome Fund Interfaces in Science Fellowship (1001774), NSF (CHE0317009), and an Institute for Biophysical Dynamics Seed Grant.

#68197 - $15.00 USD Received 28 February 2006; revised 11 April 2006; accepted 12 April 2006